Utrecht University
Faculty of Physics and Astronomy

Description and comparison of quenched jets using Q-PYTHIA simulations

B.E.J. Pelssers

July 30, 2012

Report number: UU(SAP) 12-3
Supervisors: Marco van Leeuwen and Marta Verweij

Institute of Subatomic Physics
Buys Ballot labaratory

PO BOX 80 000, 3508 TA Utrecht, The Netherlands

Contents

1 Introduction

Jets are the result of hard scattering processes between partons in high energy particle collisions. When partons with a high transverse momentum (p_T) are created, they fragment into hadrons due to quark confinement. The resulting narrow cone of high p_T particles, or jet, can then be detected. In relativistic heavy ion collisions a quark gluon plasma is formed, high p_T partons interact strongly with this plasma and lose energy, after fragmentation the resulting jet has a lower energy and different structure. These so-called quenched jets play an important role in heavy ion physics because they probe the quark gluon plasma and can be used to infer its properties.

This thesis uses Q-PYTHIA [5] to simulate quenched events. Together with simulations from unquenched events, the effect of quenching on hadron spectra, jet spectra and the behaviour of jets and dijets is studied. Several parameters are compared to data from the Large Hadron Collider. First the expected effects of quenching on jets are discussed in section 2. Section 3 gives an overview of how the simulations are done, it discusses event generation, jet finding and analysis. Section 4 is about quenched events and the effect of quenching on different spectra and jet structure. Section 5 discusses several properties of dijet events, here the dijet asymmetry is compared to ATLAS [1] data. In the last section a summary is given and conclusions are drawn, recommendations for future research are also discussed.

2 Jet Quenching

Q-PYTHIA simulates quenched events by having partons generated in proton proton collisions lose energy before hadronization. The strength of this quenching is determined by the quenching parameter $\hat{q}$ (GeV^2/fm), which quantifies the energy loss squared per femtometer. After the quenching of the event hadronization is switched back on so the partons can fragment into final state particles.

The expected result of this quenching is a suppression of high p_T particles and an increase in low p_T particles, corresponding to a shift in the p_T spectrum proportional to the quenching parameter. This suppression should be seen in spectra, such as the charged hadron spectrum, jet spectrum and intrajet spectrum. The structure of jets should also change and be observed by a larger radius and broader spatial p_T distribution. For dijet events, events where two back to back partons fragment into two jets, an asymmetry in energy should be observed because of the difference in energy loss of the partons within the medium. The angle between the two jets should deviate more from π than in unquenched events, because of the radiation of high p_T partons during quenching.

3 PYTHIA and Q-PYTHIA simulations

All simulations were done using aliroot, the ALICE optimized ROOT data analysis framework, the PYTHIA [4] and Q-PYTHIA [5] event generators and the FASTJET [6] jetfinder. First a proton-proton event is generated with a $\sqrt{s}$ of 2.76 TeV in the $0-10\%$ centrality region. For unquenched events this is done with PYTHIA, for quenched events Q-PYTHIA is used. Q-PYTHIA uses a quenching parameter $\hat{q}$ of 10 GeV^2/fm, this value is used for all simulations. Events are generated for different p_T hard bins, forcing the event generator to generate particles in a specific p_T range. During the offline analysis these different bins are added to form a complete p_T range after having been weighted to their respective cross sections. For these simulations 6 p_T hard bins were used to give a total p_T hard range of $5-120$ GeV/c. Appendix A shows a table of the different bins and their cross sections. In the final runs 2.5 million unquenched and 1 million quenched events were generated.

After event generation the generated particles are selected, all particles need to be final state hadrons in the pseudorapidity range $|\eta| < 2$. Particles can have any ϕ. Also particles need to have a p_T of at least 150 MeV. For the charged hadron spectrum only charged final state hadrons are used, for all other histograms neutral particles are included except for the neutron and K^0_{Long} because of their difficulty to be detected.

After particle selection FASTJET is used to do the jet finding using the anti-kt algorithm. The jet radius is set to 0.4, therefore all jets need to be in the $|\eta| < 1.6$ range. After jet finding all relevant parameters can be calculated and stored in their respective histograms. The online analysis consists of the scaling of the histograms, all histograms are mutiplied with the cross section of the p_T hard range and divided by the number of events and bin width.

All final runs of the simulations were done on the Nikhef Stbc computer cluster, a 256 core local batchfarm at Nikhef. A great resource to run multiple simulations with multiple p_T hard bins all at once. Therefore reducing the total time to run all simulations by a factor of 60.

After all simulations are done the different histograms are added to form one continues p_T range from 0 to 120 GeV/c. During this offline analysis the histograms are projected, selections for energies and p_T ranges are made and the quenched and unquenched data is compared.

4 Quenched events

The first spectrum looked at is the charged hadron spectrum. This spectrum includes all final state charged hadrons generated in the event and shows their transverse momentum (p_T). The spectrum is normalized to the number of events, meaning that the histogram is divided by the number of events and divided by the bin width. The distributions are shown in Figure 1.

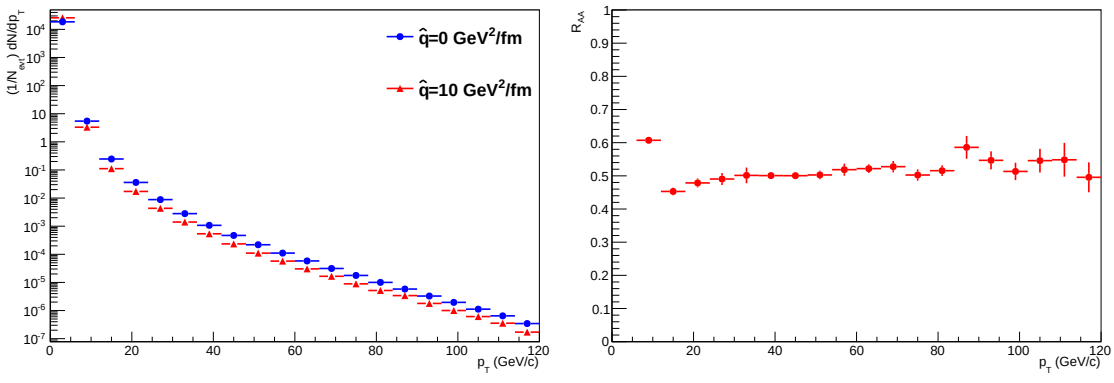

Figure 1: Spectrum of the p_T of all final state charged hadrons in the event, for $|\ \eta\ |< 2.0$.

Figure 1 shows a clear difference between the unquenched and quenched events. Both show an exponential decrease towards higher p_T as would be expected. The quenched events show an increase in low p_T particles and a suppression of high p_T compaired to the unquenched events. Dividing the two spectra yields the R_{AA} plot shown in the right panel of Figure 1 ($\hat{q}$ = 10 GeV^2/fm events divided by $\hat{q} = 0$ GeV^2/fm events). The R_{AA} is an almost constant 0.5 with a very slight increase towards higher p_T , corresponding to an energy loss due to quenching. The R_{AA} at very low p_T (below 5 GeV/c) is extremely high because it is outside the PYTHIA p_T hard range and therefore not accurately calculated.

Measurements by ALICE [3] and CMS [2] allow the simulations te be compared to LHC data. Both ALICE and CMS show a minimum $R_{AA} \approx 0.15$ at $p_T = 6$ GeV/c which rises to $R_{AA} \approx 0.35$ at $p_T = 19$ GeV/c (ALICE), and to $R_{AA} \approx 0.6$ at $p_T = 70$ GeV/c (CMS). This is clearly not observed in the simulations. Q-PYTHIA is not capable of reconstructing the charged hadron spectrum properly. However, the following sections will show that this is not a problem with jets.

The energy loss observed in the R_{AA} histogram shows a shift of the spectrum to lower p_T. The shift in Figure 1 seems to be about one bin width, which would mean a p_T shift of 6 GeV/c. Because the R_{AA} deviates greatly from the LHC data, the energy shift is not calculated for Figure 1. For the jet spectrum in subsection 4.1 it is calculated.

4.1 Jet spectra

By looking at the jet spectrum the same shift to lower p_T should be visible for the quenched events. Figure 2 shows that this is indeed the case. It shows the p_T of all jets in the event for $|\eta| < 1.6$, since the jet radius was set to 0.4 and particles are all within $|\eta| < 2$. All final state hadrons are used for jet finding except for neutrons and K^0_L particles. These two particles are

discarded because they are not detectable and could therefore make it harder to compare the simulations to actual data.

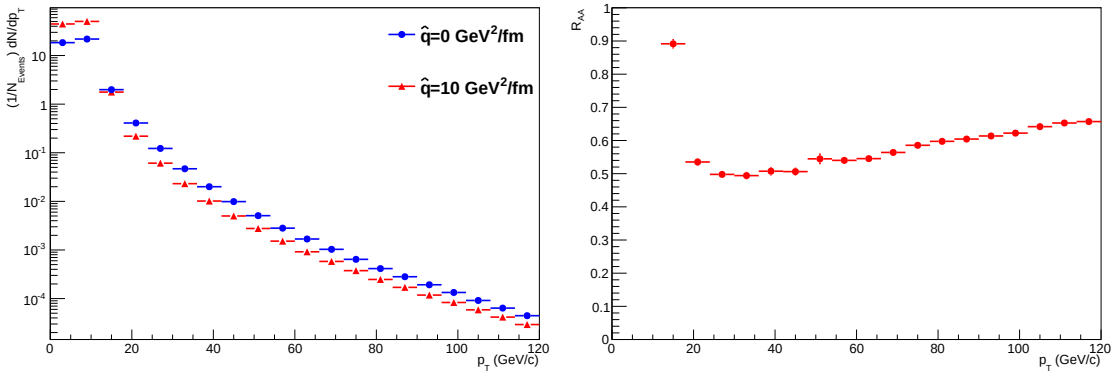

Figure 2: Spectrum of the p_T of jets

Figure 2 again shows a clear difference between the unquenched and quenched events, both of which have a peak at about $p_T = 10$ GeV/c, the minimum jet energy. Analogous to the hadron spectra, there is a suppression of high p_T jets from the quenched events but the rising R_{AA} shows that this suppression decreases significantly for higher p_T jets. From 0.50 at 30 GeV/c the R_{AA} increases to 0.66 at 120 GeV/c. This shows there is less energy loss at higher p_T because of a higher jet collimation giving fewer out-of-cone particles (More on jet collimation in section 4.3).

Instead of comparing the quenched to the unquenched jets by looking at the R_{AA}, the spectra can also be compaired by shifting the quenched spectrum and calculating the energy loss associated with this shift. By first fitting the unquenched spectrum to the fitting function $f(p_T) = \frac{c1}{p_T^6} + c2$ and determining the fitting parameters $c1$ and $c2$ an unquenched fit is obtained. This function can then be fitted to the quenched spectrum by using $p'_T = p_T(1 - \epsilon_f)$ to give a fractional p_T dependent energy loss ϵ_f. Or $p'_T = p_T - \epsilon_a$ to give an absolute p_T independent shift ϵ_a. Doing this analysis gives $\epsilon_f = -0.088 \pm 0.001$ and $\epsilon_a = -5.28 \pm 0.07$ GeV/c. The fractional energy loss for the quenched jets is 8.8% compared to the unquenched jets, or equivalently the absolute energy loss for quenched jets is 5.28 GeV/c. The energy loss is probably p_T dependent, because of the rising R_{AA} in figure 2. However the fit using the $p'_T = p_T(1 - \epsilon_f)$ method has a higher χ^2 compared to $p'_T = p_T - \epsilon_a$. The first having a $\chi^2 = 175.17$ and the second a $\chi^2 = 12.41$.

4.2 Momentum distribution in jets

Simulations of the intrajet particle p_T distribution give information about the internal jet structure. Particularly about the R_{AA} in different p_T domains and different $p_{T,Jet}$ domains. The same parameters for particle selection used in the jet spectra were also used for these intrajet spectra. Figure 3 shows the intrajet spectra in three different $p_{T,Jet}$ regions. First the complete range (0 GeV/c to 120 GeV/c), then the mid range of the $p_{T,Jet}$ range (40 GeV/c to 60 GeV/c) and lastly the high $p_{T,Jet}$ range (100 GeV/c to 120 GeV/c).

There is a suppression of the particle yield in all three $p_{T,Jet}$ regions. The R_{AA} of the complete spectrum is close to 0.3, with a slight decrease at the high p_T end. In the 40 to 60 GeV/c $p_{T,Jet}$ range the same is observed. In the high 100 to 120 GeV/c $p_{T,Jet}$ range however the R_{AA} is at

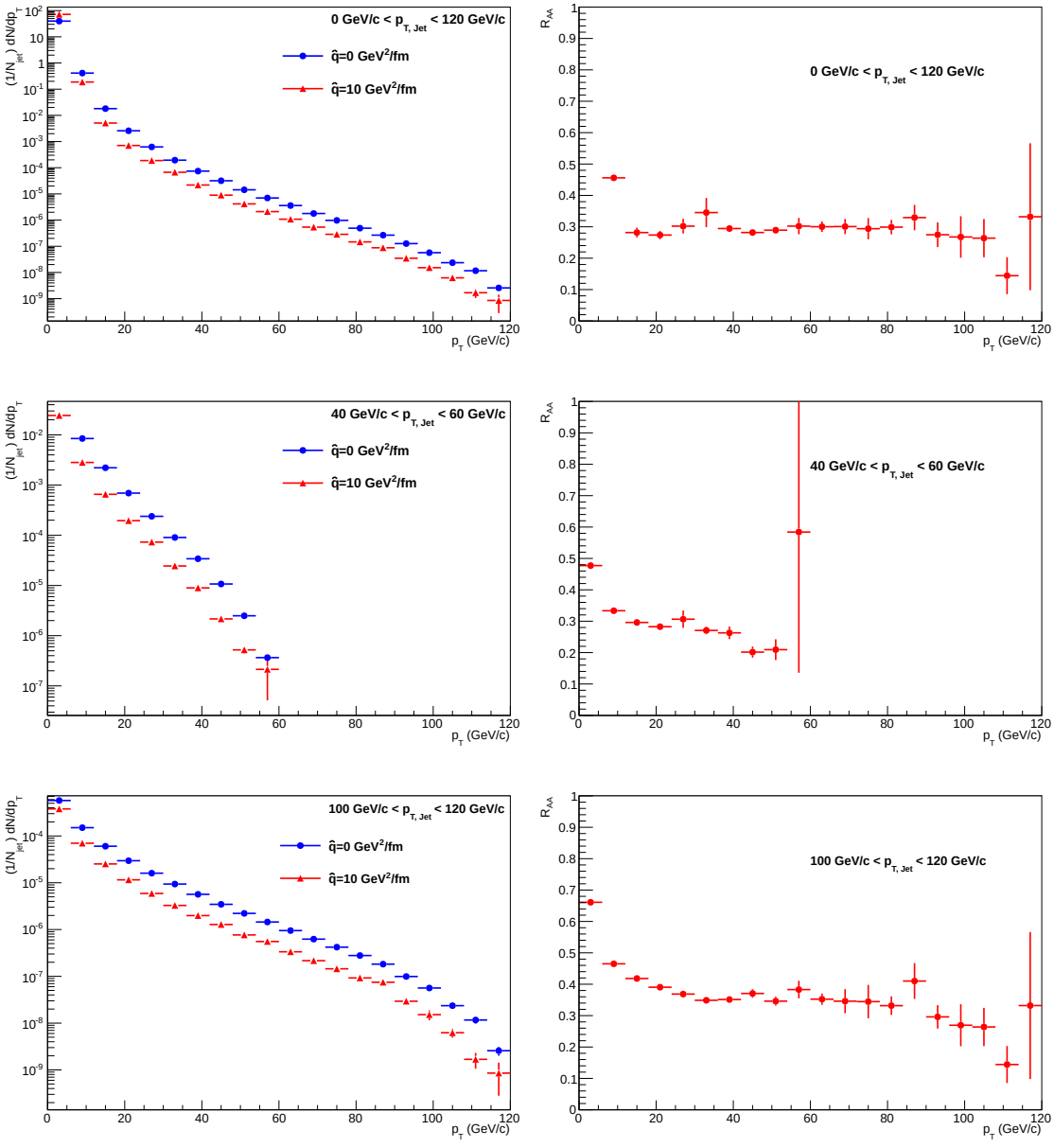

Figure 3: Intrajet spectra and their R_{AA}'s for three different $p_{T,Jet}$ ranges; the full spectrum (0 to 120 GeV/c), the mid region (40 to 60 GeV/c) and the high end (100 to 120 GeV/c).

0.4, but with a decrease at high p_T and an increase towards lower p_T.

Quenching produces more low p_T particles and less particles with high p_T as can be seen by the increasing R_{AA} at low p_T and the decreasing R_{AA} at high p_T.

4.3 Jet structure

In subsection 4.1 it was concluded that the decrease in quenching of high p_T particles was due to higher collimated jets, to see whether this is really the case the radius r of all intrajet particles is calculated. This is done in the same simulation as for the intrajet spectrum, so the same parameters are used. The radius is defined as:

$$r = \sqrt{(\phi_{Particle} - \phi_{Jet})^2 + (\eta_{Particle} - \eta_{Jet})^2}$$

The jet radius is set to 0.4 in FASTJET, so all particles are expected to have an r between 0 and 0.4. Lastly the histogram is scaled to the number of particles per jet. Two $p_{T,Jet}$ regions are shown in figure 4.

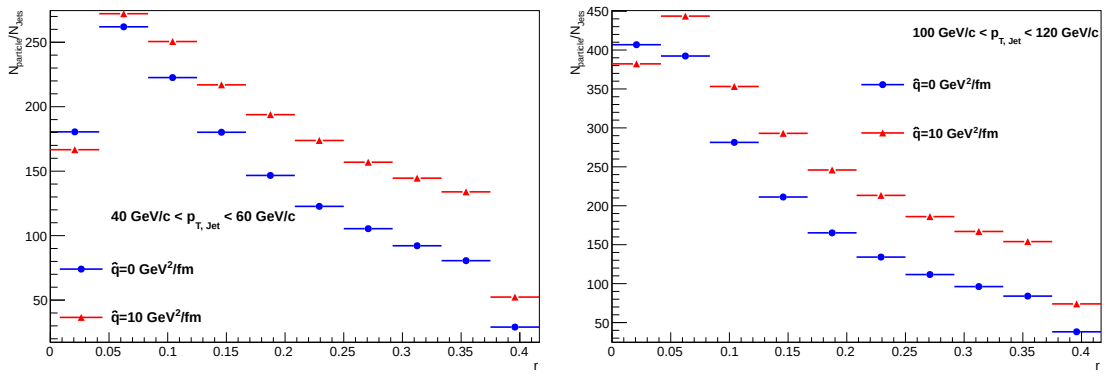

Figure 4: Two plots of the radii of intrajet particles, for the 40 to 60 GeV/c $p_{T,Jet}$ range and 100 to 120 GeV/c $p_{T,Jet}$ range.

When compairing the two $p_{T,Jet}$ ranges it can be seen that higher p_T jets are more collimated. The peak in both quenched and unquenched events in the left panel of figure 4 is shifted to lower r in the right panel. In both panels the quenched distribution is shifted to the right, meaning there are more particles at with higher r. Quenching causes some of the particles to go out-of-cone, these particles with an $r > 0.4$ are not reconstructed in the final jets.

The differential p_T distribution in figure 5 shows how the p_T of the intrajet particles is distributed as a function of r. Again for $p_{T,Jet} = 20$ GeV/c and for $p_{T,Jet} = 100$ GeV/c.

Figure 5 shows that for higher $p_{T,Jet}$ the distribution rises more steeply, meaning a more collimated jet as the energy is more concentrated in the center region. For $p_{T,Jet} = 100$ GeV/c 75% of the energy is contained in the area $r < 0.2$, whereas for $p_{T,Jet} = 20$ GeV/c this is only 60%. In both cases the quenched jets have a more gradual p_T distribution, meaning that the energy is not as concentrated as the unquenched case.

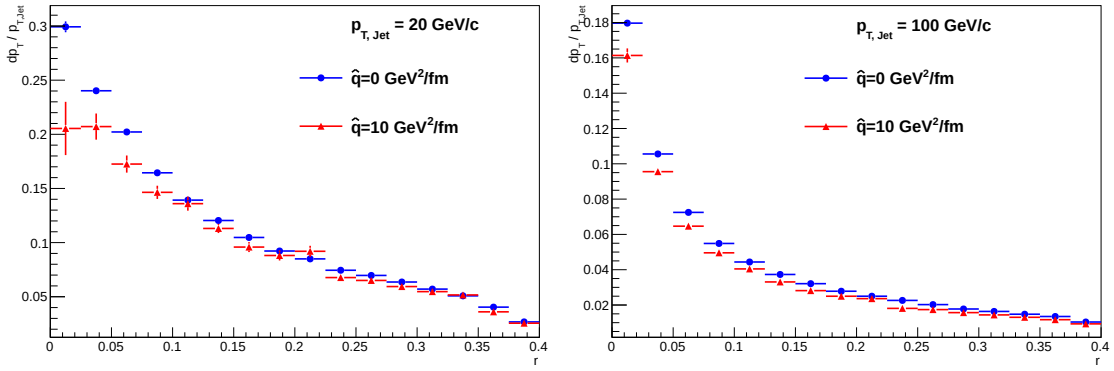

Figure 5: Histogram of the differential p_T distribution $dp_T/p_{T,Jet}$ for $p_{T,Jet} = 20$ GeV/c and $p_{T,Jet} = 100$ GeV/c.

5 Dijet events

There are several ways to quantify the structure of dijet events, this thesis uses the energy asymmetry of the dijet A_J, the angle between the leading and secondary jet $\Delta\phi$ and lastly the imbalance in jet momenta p_{T2}/p_{T1}. The first two methods are also used by ATLAS [1], the latter by CMS. Therefore making it possible to compare the results of the simulated events to LHC data. Lastly there will be a subsection about multijet events where possible three jet events will be discussed.

5.1 Dijet asymmetry

The dijet asymmetry of two jets with energies E_{T1} and E_{T2} is given by:

$$A_J = \frac{E_{T1} - E_{T2}}{E_{T1} + E_{T2}}$$

A further requirement is that these two jets need to be in opposite hemispheres, or $\Delta\phi > \frac{\pi}{2}$. Lastly to select high p_T jets the leading jet is required to have a minimum energy $E_{T1} > 55$ GeV. The secondary jet a minimum of $E_{T2} > 25$ GeV to discard any soft background. Unfortunately these energy thresholds are not as high as those used by ATLAS ($E_{T1} > 100$ GeV, $E_{T2} > 25$ GeV), because of the p_T hard range used in PYTHIA. Still they are large enough to clearly show jet quenching. The resulting histogram is scaled to the number of jet-selected events, meaning all dijet events that meet the energy selection and where $|\eta_{Jet}| < 1.6$. The result is shown in figure 6.

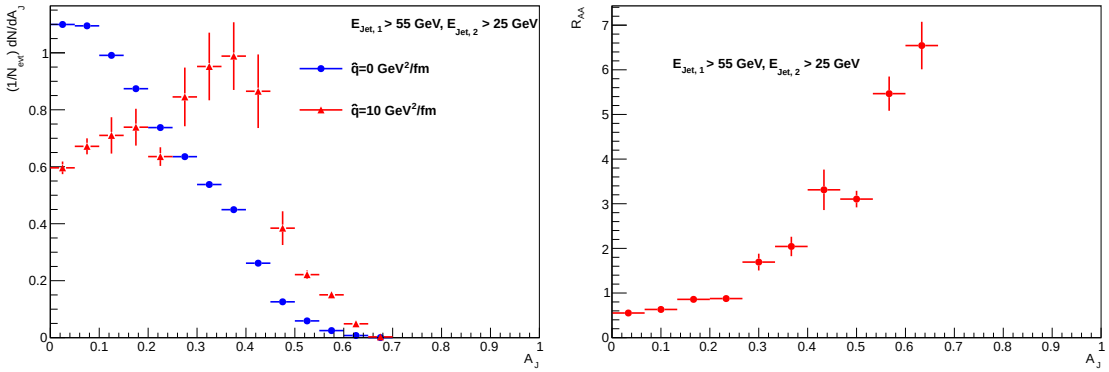

Figure 6: Asymmetry distribution of dijet events using PYTHIA and Q-PYTHIA. Both absolute and R_{AA} plots are shown.

The asymmetry distribution of the quenched jets shows a clear shift towards higher asymmetry, with a mean of 0.27 compared to a mean of 0.19 for unquenched jets. Something that is also seen in the R_{AA} plot, which shows a suppression of low asymmetry jets and a continues increase towards higher values.

These simulations are compared to data obtained by ATLAS, which results in figure 7. Here the energy selection is changed to best fit the ATLAS p+p data, all other parameters are kept the same.

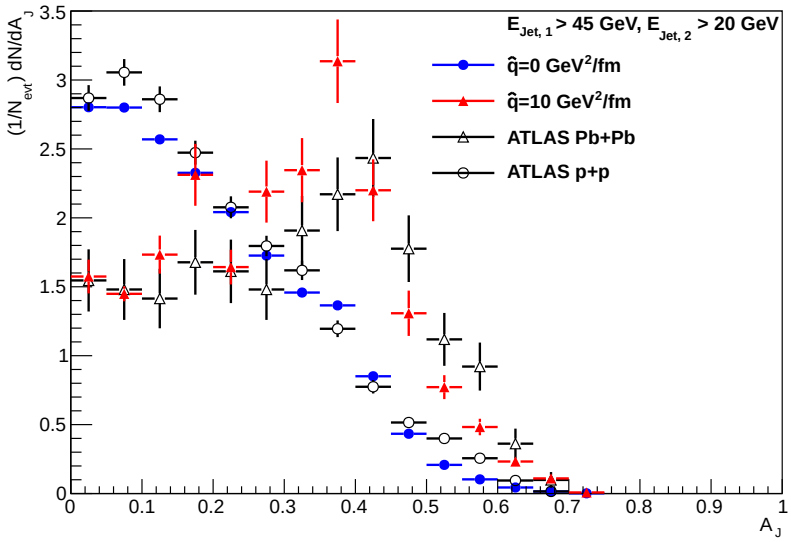

Figure 7: Dijet asymmetry of quenched and unquenched jets superimposed on ATLAS data. $\sqrt{s_{NN}} = 2.76$ TeV for Pb+Pb data and $\sqrt{s} = 7$ TeV for p+p.

Figure 7 shows the same behaviour for unquenched en proton data. The quenched and lead-lead data is not as good, but shows the same shift towards higher asymmetry. There are several reasons for the discrepancies between the quenched and lead-lead data; first, due to the Q-PYTHIA p_T range chosen for the simulations, the energy selection can not be as high as the range used by ATLAS. Second, the $\hat{q}$ value is not optimized to fit the data, it was merely chosen to clearly show the effect of quenching. Nevertheless the simulations show that quenched jets behave similarly compared to jets in heavy-ion collisions.

5.2 Dijet angular correlations

Event selection for the angular correlations has the same criteria as for the dijet asymmetry except for the energy selection. The correlations are shown in figure 8. $\Delta\phi$ is defined as: $\Delta\phi = \phi_{SecondJet} - \phi_{LeadingJet}$. Jets need to be in opposite hemispheres, or $|\Delta\phi| > \frac{\pi}{2}$. If $\Delta\phi > \pi$, than $2\pi - \Delta\phi$ is taken as the angle between the jets.

Figure 8 shows the resulting histogram of the angular correlations. ATLAS data is also included. The unquenched spectrum follows an exponential decline to lower $\Delta\phi$ showing that the majority of the dijets are almost back to back as was to be expected. The quenched jets show an increase at low $\Delta\phi$ and an decrease in the high $\Delta\phi$ range. Meaning less back to back jets and more jet dispersion due to quenching. The figure also shows the comparison of the simulations with ATLAS data, again with 7 TeV proton data and 2.76 TeV lead-lead data. As with the previous asymmetry plots, the energy selection is chosen to best fit the proton data to the unquenched simulations.

Figure 8 shows the same behaviour for proton data and unquenched events. The lead data shows the same increase in low $\Delta\phi$ dijets as the quenched simulations, leading to the conclusion that quenched jets show the same angular correlation as jets from lead-lead collisions.

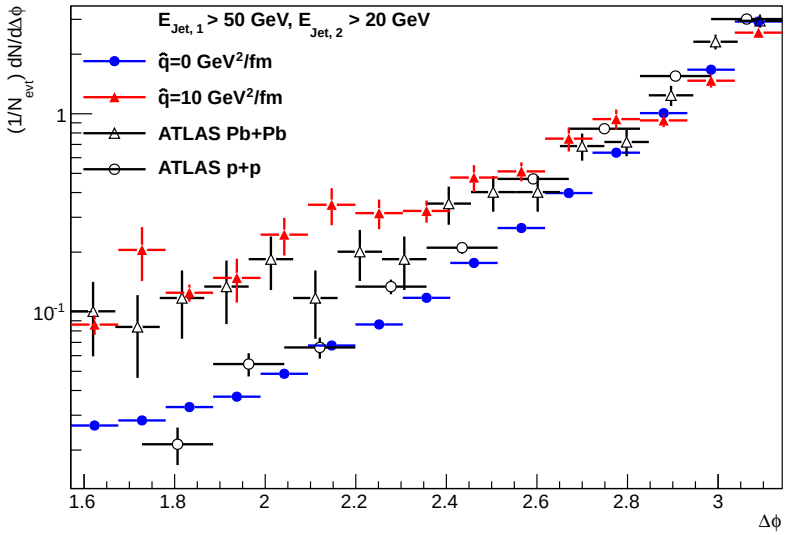

Figure 8: Dijet angular correlation between leading and second jets, compaired to ATLAS data, $\sqrt{S_{NN}} = 2.76$ TeV for Pb+Pb data and $\sqrt{s} = 7$ TeV for p+p.

5.3 Dijet momentum imbalance

Another way to look at the quenching of dijets is to look at the p_T imbalance of the jets. For a dijet with jet momenta $p_{T,1}$ for the leading jet and $p_{T,2}$ for the second jet the imbalance is simply $p_{T,2}/p_{T,1}$. Figure 9 shows the result of the simulation, the same parameters were used as in the $\Delta\phi$ and A_J simulations. The only selection is the p_T range of the leading jet. For the p_T of the second jet, there is only a minimum p_T to get rid of any soft background. Here the leading jets have momenta between 100 and 120 GeV/c and the second jets a minimum p_T of 30 GeV/c.

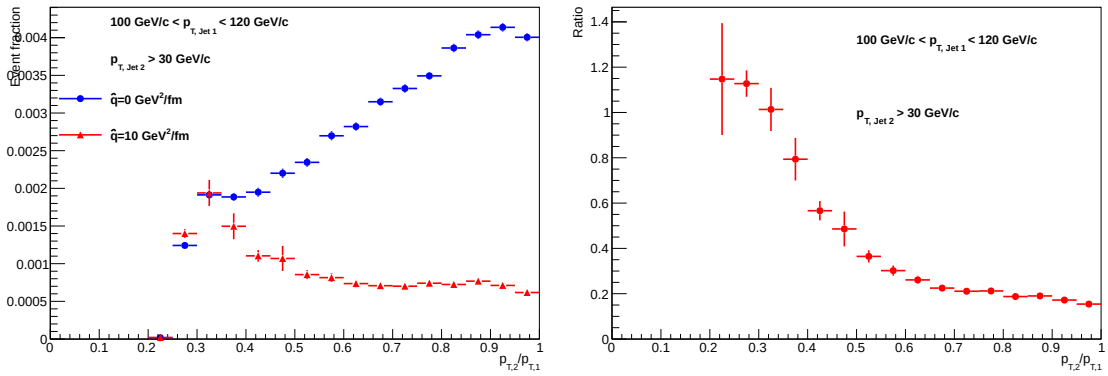

Figure 9: Dijet imbalance for leading jets between 100 and 120 GeV/c and second jets of at least 30 GeV/c.

The unquenched events in figure 9 show a peak at high $p_{T,2}/p_{T,1}$ meaning that most jets have comparable p_T and are balanced. After seeing the A_J and $\Delta\phi$ plots this is to be expected. The spectrum decreases towards lower $p_{T,2}/p_{T,1}$ and falls of completely at a $p_{T,2}/p_{T,1}$ of 0.25. The quenched case shows a dramatic decrease in high $p_{T,2}/p_{T,1}$ events meaning that most quenched dijets are far out of balance. The R_{AA} plot shows how the R_{AA} decreases from just above 1 at the low $p_{T,2}/p_{T,1}$ end to 0.2 at the high $p_{T,2}/p_{T,1}$ end, again showing the asymmetry between the two dijets.

5.4 Multijet events

After studying the angular correlations of dijets, there is reason to assume that quenched events in the lower $\Delta\phi$ region, below $\Delta\phi < 2.6$, are three-jet events. The reason being that for small $\Delta\phi$ the radiated parton has a large enough p_T to fragment into the third jet.

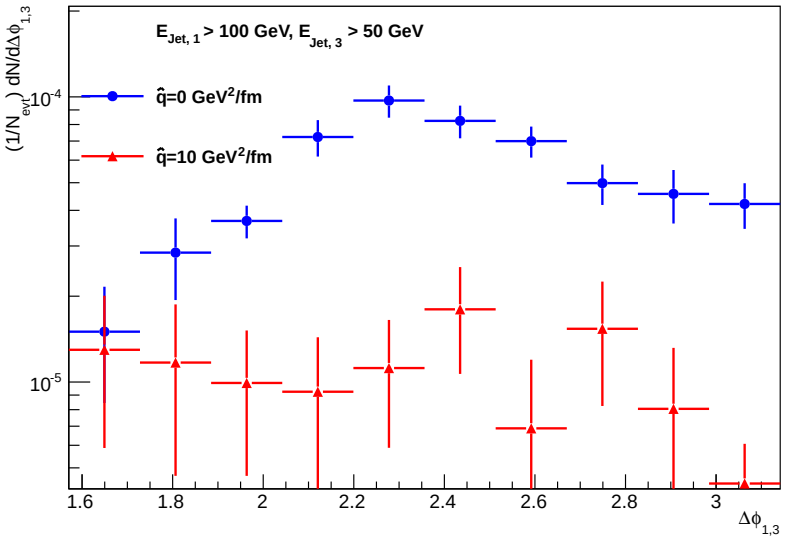

Figure 10: Leading to third jet angular correlations.

Figure 10 shows the angle $\Delta\phi_{1,3}$ between the leading and third jet, the histogram is normalized to the number of three-jet events and used the same parameters as for the $\Delta\phi$ histogram in figure 8, except for the dijet event selection. Only events where the angle between the leading and second jet is smaller than 2.6 are used. The leading jet is required to have a minimum p_T of 100 GeV/c, the third jet a minimum of 50 GeV/c. The unquenched case shows a peak at $\Delta\phi_{1,3} \approx 2.3$, a typical angle for third jets. The quenched spectrum however has a lot less events and does not have any clear peaks, it does fall off when $\Delta\phi_{1,3}$ goes towards π. Therefore quenching does not seem to cause more three-jet events in the low $\Delta\phi_{1,2}$ region, but instead causes existing three-jet events to lose energy which in turn dissipates the third jets almost completely.

6 Conclusions

In all simulations the effects of quenching are clearly visible. The hadron spectrum, jet spectrum and intrajet spectrum all show a suppression of high p_T particles and the different R_{AA} histograms show the different energy loss. For the jet spectra the shift in p_T shows a p_T dependent energy loss. Jet structure is also affected by quenching, as can be seen in the Σp_T histograms, resulting in less collimated jets and a broader spatial p_T distribution. The study of dijets shows a good agreement between unquenched events and ATLAS proton data, whereas quenched events shows similarities with ATLAS lead-lead data. Showing a relation between heavy ion collisions and quenching. Lastly three-jet events were studied, these reveal that quenching does not produce more jets in the low $\Delta\phi$ region, but rather dissipates already existing third jets.

Overall it can be said that Q-PYTHIA offers good simulations of quenched events, except for the charged hadron spectrum all spectra and parameters show the expected quenching. Comparing the simulations to LHC data shows similar behaviour of quenched events and heavy ion collisions, implying that the underlying physics is the same.

6.1 Discussion and future research

This thesis has used a $\hat{q}$ value of 10 GeV^2/fm for all simulations, this value was chosen to clearly show the effect of quenching, not for quantitative purposes. When comparing the dijet asymmetry to ATLAS data, it was seen that the quenched events agreed roughly with the data. However the $\hat{q}$ value is most likely not the most optimal one, therefore future research might use different $\hat{q}$ values to find a better fit. Different $\hat{q}$ values might also be used to study the energy loss in jet spectra. In section 4.1 the fractional energy loss ϵ_f and the absolute loss ϵ_a were determined. Future research might determine these energy losses for different $\hat{q}$ values to find a possible relation between ϵ and $\hat{q}$. Further research might include more and higher p_T hard bins, again to get better fits with ATLAS data and to also compare CMS data to the $p_{T,2}/p_{T,1}$ histograms. Lastly several other parameters that were kept constant in these simulations could be varied, for example by looking at different centrality regions or a different jet radius to study the influence of out-of-cone radiation.

References

[1] G. Aad *et al.* PRL 105,252303 (2010) *Observation of a Centrality-Dependent Dijet Asymmetry in Lead-Lead Collisions at* $\sqrt{S_{NN}} = 2.76$ *TeV with the ATLAS Detector at the LHC* December 17, 2010

[2] S. Chatrchyan *et al.* [CMS Collaboration], *"Study of high-pT charged particle suppression in PbPb compared to pp collisions at sqrt(sNN)=2.76 TeV,"* Eur. Phys. J. C **72** (2012) 1945 [arXiv:1202.2554 [nucl-ex]].

[3] ALICE Collaboration: K. Aamodt, *et al.* arXiv:1012.1004v1 [nucl-ex] December 5, 2010

[4] T. Sjostrand, S. Mrenna and P. Skands, JHEP05 (2006) 026 (LU TP 06-13, FERMILAB-PUB-06-052-CD-T) [hep-ph/0603175]

[5] Néstor Armesto, Leticia Cunqueiro and Carlos A. Salgado arXiv:0907.1014v1 [hep-ph] *Q-PYTHIA: a medium-modified implementation of final state radiation* July 6, 2009

[6] M. Cacciari, G.P. Salam and G. Soyez Phys. Lett. B641 (2006) [hep-ph/0512210]

[7] Clint Young, Björn Schenke, Sangyong Jeon and Charles Gale arXiv:1103.5769v2 [nucl-th] *Dijet asymmetry at the Large Hadron Collider* June 3, 2011

A Cross sections of p_T hard bins

The following table lists the different total cross sections for the different p_T hard bins used. The cross section decreases for higher p_T showing the usefullness of different p_T hard bins to generate high p_T particles.

p_T hard bin number	$p_{T,min}$ (GeV/c)	$p_{T,max}$ (GeV/c)	Total cross section (mb)
1	5	10	11.60
2	11	25	$6.514 \cdot 10^{-1}$
3	26	40	$1.656 \cdot 10^{-2}$
4	41	60	$2.115 \cdot 10^{-3}$
5	61	85	$3.121 \cdot 10^{-4}$
6	86	120	$5.716 \cdot 10^{-5}$

Table 1: Total cross sections for each $p_T$hard bin.